Available online at www.sciencedirect.com

SciVerse ScienceDirect

Acta Materialia xxx (2012) xxx–xxx

Acta MATERIALIA

www.elsevier.com/locate/actamat

Plastic deformation of NiTi shape memory alloys

Tawhid Ezaz [a], J. Wang [a], Huseyin Sehitoglu [a,*], H.J. Maier [b]

[a] Department of Mechanical Science and Engineering, University of Illinois at Urbana-Champaign, 1206 W. Green St., Urbana, IL 61801, USA
[b] University of Paderborn, Lehrstuhl für Werkstoffkunde, D-33095 Paderborn, Germany

Received 13 December 2011; received in revised form 6 September 2012; accepted 9 September 2012

Abstract

Dislocation slip in B2 NiTi is studied with atomistic simulations in conjunction with transmission electron microscopy (TEM). The atomistic simulations examine the generalized stacking fault energy (GSFE) curves for the $\{0\,1\,1\}$, $\{\bar{2}\,1\,1\}$ and $\{0\,0\,1\}$ planes. The slip directions considered are $\langle 1\,0\,0\rangle$, $\langle 1\,1\,1\rangle$ and $\langle 0\,1\,1\rangle$. The results show the smallest energy barriers for the $(0\,1\,1)[1\,0\,0]$ case, which is consistent with the experimental observations of dislocation slip reported in this study. To our knowledge, slip on the $(0\,1\,1)[1\,\bar{1}\,1]$ system is illustrated for the first time in our TEM findings, and atomistic simulations confirm that this system has the second lowest energy barrier. Specimens that underwent thermal cycling and pseudoelasticity show dislocation slip primarily in the austenite domains while the bulk of martensite domains does not display dislocations. The results are discussed via calculation of the ideal slip nucleation stress levels for the five potential slip systems in austenite.

Keywords: Shape memory; Slip; NiTi; Dislocations; Density functional theory

1. Introduction

The shape memory alloy NiTi has considerable technological relevance and has also been scientifically perplexing. For some time, the plastic deformation of austenite via dislocation slip has not been fully understood, although it is very important as it limits the shape memory performance [1–6]. The role of slip in austenite has drawn significant attention recently [7–10].

The understanding of NiTi has been empowered with recent atomistic simulations. The simulations provide the energy levels for the different phases [11–13], the lattice parameters [14], the elastic constants [15] and the energy barriers for martensite twinning [16,17]. Beyond these advances, a detailed consideration of the dislocation slip behavior via simulations is urgently needed to compare with the experimental findings of active slip systems. Upon establishing the GSFE (generalized stacking fault energy) curves in the austenitic (B2) phase, we study the propensity of five potential slip systems, and note the formation of anti-phase boundaries (APBs) in certain cases. Consequently, we assess the magnitude of ideal stresses needed to activate slip in these different systems. We find the $(0\,1\,1)[1\,0\,0]$ system to be the most likely one consistent with experiments. The occurrence of $(0\,1\,1)[1\,\bar{1}\,1]$ slip is reported in our experimental findings in Section 2.1, which has not been reported earlier to our knowledge. This is the second most likely slip system after $[1\,0\,0]$ slip.

To gain a better appreciation of the role of slip on shape memory behavior we show two results in Fig. 1 for NiTi. In the first case, the temperature is cycled at a constant stress (Fig. 1a). The range of temperature is 100 to −100 °C, which is typical for application of NiTi. It is evident that as the stress magnitudes exceed 150 MPa, the strain upon heating is not fully recoverable. A small plastic strain remains and this is primarily due to residual dislocations in the B2 matrix. In Fig. 1b the experiment is conducted at a constant temperature. The sample is deformed and austenite-to-martensite transformation occurs, with

* Corresponding author. Tel.: +1 217 333 4112; fax: +1 217 244 6534.
E-mail address: huseyin@illinois.edu (H. Sehitoglu).

1359-6454/$36.00
http://dx.doi.org/10.1016/j.actamat.2012.09.023

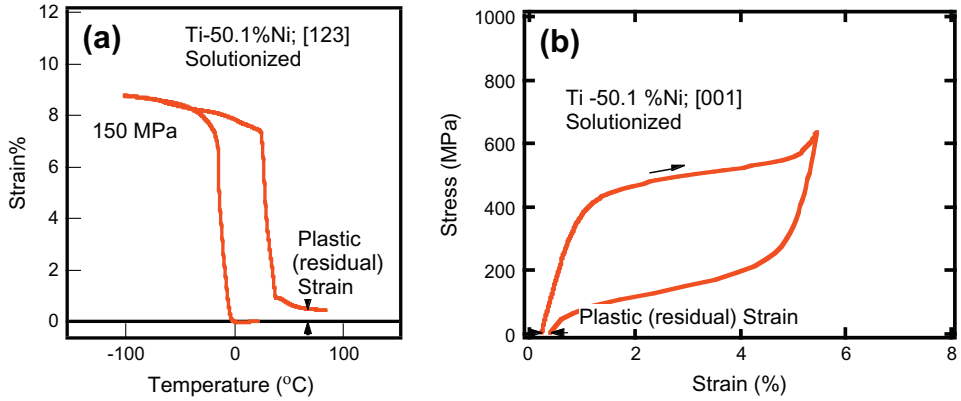

Fig. 1. Shape memory and pseudoelasticity experiments on solutionized 50.1% Ni–Ti: (a) The development of macroscopic plastic (residual) strain upon temperature cycling (100 °C to −100 °C) under constant stress [18], (b) the plastic (residual) strain under pseudoelasticity at constant temperature ($T = 28$ °C).

austenite domains primarily undergoing dislocation slip to accommodate the transformation strains (see Section 2.2 for further details). Upon unloading, a small but finite amount of plastic strain remains. The plastic strains become noticeable at the macroscale at stress levels exceeding 600 MPa for the solutionized 50.1% Ni NiTi. The small plastic strains can accumulate over many cycles and deteriorate the shape memory effect. Apart from the residual strain that is produced, the presence of plasticity reduces the maximum transformation strain and increases the stress hysteresis, two other measures of shape memory performance. This will be discussed further in Section 2.3.

Under fatigue loading, the NiTi alloys exhibit gradual degradation of pseudoelasticity with cycles, and this deterioration has been attributed to slip deformation [3,4]. As stated above, the domains that undergo slip curtail the reversibility of transformation. Therefore, a higher slip resistance is desirable to achieve pseudoelasticity over many cycles in NiTi. Based on this background, it is extremely worthwhile to develop a quantitative understanding of dislocation slip; specifically, it is crucial to determine the energy barriers (GSFE curves) for the most important slip systems. In this study, the simulation results (in Sections 3 and 4) are aimed towards building a framework for a better comprehension of shape memory alloys.

The glide planes and directions of possible slip systems in austenitic NiTi are shown in Fig. 2. We note that there are multiple planes within the same family of slip systems, and only one of the planes is shown in Fig. 2 for clarity. The potential slip planes are $\{011\}$, $\{\bar{2}11\}$ and $\{001\}$. In the studies of Chumlyakov et al. [7] and Tyumentsev et al. [18], NiTi is deformed at high temperatures (>473 K) where slip dominates. The slip systems were identified as $\{110\}\langle010\rangle$ and $\{100\}\langle010\rangle$. The $\{110\}\langle010\rangle$ system was proposed by Moberly et al. [19]. More recently, Simon et al. [8], and Norfleet et al. [9] provided details of "transformation-induced plasticity" and indexed the $\{101\}\langle010\rangle$ slip system. The "transformation-induced plasticity" refers to the nucleation and build-up of slip in austenite to accommodate the rather high transformation strains [20–22] upon traversing martensite interfaces [22]. Recently, Delville et al. [23] argued the source of the irreversibility in shape memory alloys as primarily slip deformation; we note that residual martensite can also prevail, and contribute to the irreversibility.

NiTi alloys exhibit considerable ductility. This high ductility behavior is viewed as unusual since B2 intermetallic alloys are expected to exhibit limited ductility [24]. As discussed above, the $\{011\}\langle100\rangle$ permits glide only in three independent slip systems. The presence of only three independent systems for the $\{011\}\langle100\rangle$ case was discussed in the textbook by Kelly et al. [25] and more recently in a paper on NiTi by Pelton et al. [10]. If loading was applied at any point along the cube axis the cube is not able to deform because the resolved shear stress is zero for all possible $\langle100\rangle$ directions, hence certain orientations produce no glide if there are less than five independent slip systems. Given that at least five independent slip systems are required for dislocations to accommodate arbitrary deformations [26], additional slip systems must be present in B2 NiTi, contributing to the enhanced plasticity. In B2 alloys, the potentially operative $\{110\}\langle111\rangle$ slip provides an additional nine deformation modes that can contribute significantly to the superior ductility. The slip system $\{110\}\langle111\rangle$, though observed in a few ordered intermetallic alloys of B2 type such as β-CuZn [27] and FeCo [28], has, however, not been reported for NiTi to our knowledge. Rachinger and Cottrell [29] classified the B2 type intermetallic compounds to two categories: (i) those of ionic binding with slip direction in $\langle100\rangle$ and (ii) those dominated by metallic binding with slip direction $\langle111\rangle$. In this paper, we report experimental evidence with transmission electron micrographs of $\{110\}\langle111\rangle$ slip in B2 NiTi in Section 2, and provide an energetic rationale in comparison to the other possible B2 slip modes such as (011) $[0\bar{1}1]$, $(001)[010]$ and $(\bar{2}11)[111]$ in Section 4.

The underlying basis of dislocation motion in a certain glide plane and direction is described by the generalized stacking fault energy curve (GSFE) [30]. Simulations incorporating electronic structure are capable of predicting

Please cite this article in press as: Ezaz T et al. Plastic deformation of NiTi shape memory alloys. Acta Mater (2012), http://dx.doi.org/10.1016/j.actamat.2012.09.023

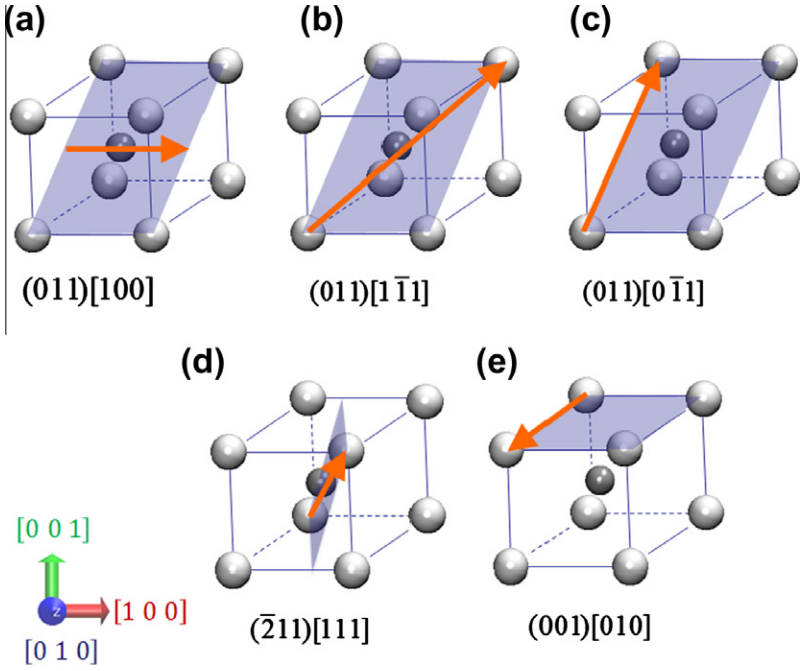

Fig. 2. Glide planes and directions of different possible slip systems in austenitic NiTi. The shaded violet area points to the glide plane and the orange arrow shows the glide direction in (a) (011)[100], (b) (011)[1 $\bar{1}$ 1], (c) (011)[0 $\bar{1}$ 1], (d) ($\bar{2}$11)[111] and (e) (001)[010] systems respectively. (For interpretation of the references to colour in this figure legend, the reader is referred to the web version of this article.)

which systems are most likely. We also discuss dislocation dissociation scenarios for the ⟨1 1 1⟩ slip system in Section 5, uncovering the energetic basis (GSFE) of the superpartials formed via dissociations with lower energy barriers.

Specifically, we focus on the (0 1 1)[1 0 0], (0 1 1)[1 $\bar{1}$ 1], (0 0 1)[0 1 0], (0 1 1)[0 $\bar{1}$ 1] and ($\bar{2}$ 1 1)[1 1 1] dislocation slip cases. This information is critical for micro-mechanical models at higher length scales that can be used to predict the mechanical response during service as well as during processing. We also report transmission electron micrographs providing evidence of (0 1 1)[1 $\bar{1}$ 1] glide in conjunction with (0 1 1)[1 0 0] slip from experiments under numerous experimental conditions. Our quantitative GSFE calculations provide an underlying rationale for these observations and will be discussed in detail in this paper.

2. Experimental results

2.1. Experimental evidence of {0 1 1}⟨1 0 0⟩ and (0 1 1)⟨1 $\bar{1}$ 1⟩ slip

To determine the slip planes and slip directions, experiments were conducted under compression at room temperature (28 °C) on solutionized single crystals of 50.1% Ni NiTi. The solutionized (SL) samples underwent heating to 940 °C for 24 h and then quenching. In this case, the austenite finish temperature is 10 °C while the martensite finish

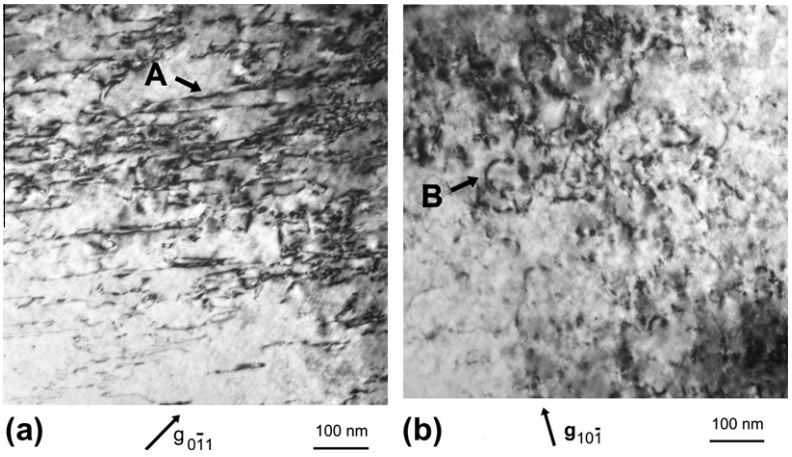

Fig. 3. (a) Transmission electron micrographs of dislocations in the specimen deformed at room temperature imaged with different g-vectors. The black arrow labeled with black letter A points to dislocations of the ⟨1 0 0⟩ type and (b) shows dislocations of the ⟨1 $\bar{1}$ 1⟩ type (labeled with black letter B).

temperature is near −40 °C. In Ref. [31], the DSC curves for other heat treatments are provided.

The mechanical response of the deformed sample is shown in Fig. 1b. In the case examined in this work, the specimen is subjected to compression in the [0 0 1] direction to strain levels of 5% and unloaded to zero stress. A very small residual plastic strain is present upon unloading and does not recover upon heating (Fig. 1b). The overall behavior is pseudoleastic at the macroscale; however, dislocations are observed at the microscale.

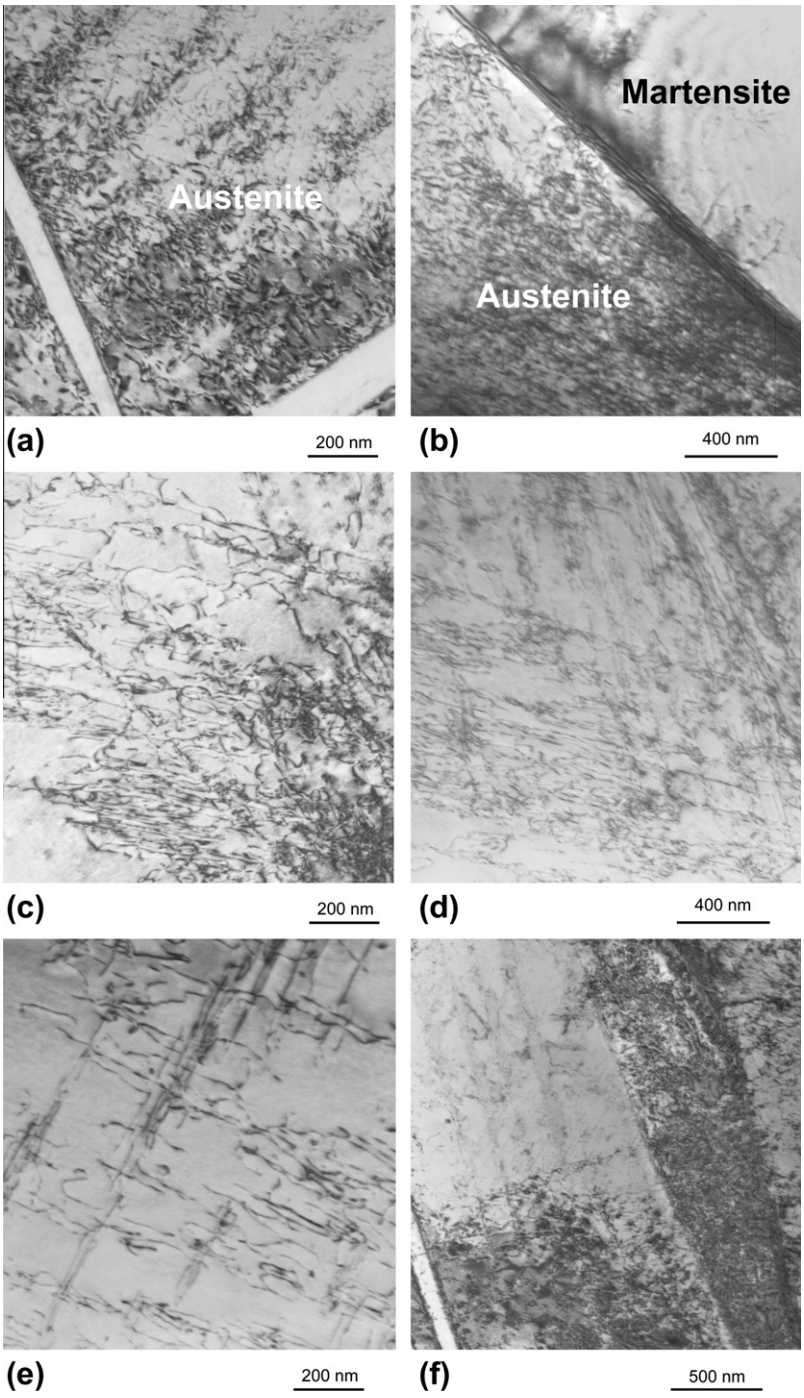

Fig. 4. (a, b) TEM images of a solutionized Ti–50.4 at.% Ni [1 2 3] single crystal taken at room temperature which was thermomechanically tested under constant uniaxial tensile load while the temperature was cycled from RT → −100 °C → 100 °C → RT. The load was increased in 25 MPa increments from 0 MPa to 100 MPa in successive tests. (c) TEM image from a 50.1% Ni single crystal of [1 1 1] orientation thermally cycled under constant load (1 cycle at each + 10 MPa increment from +100 MPa to +170 MPa) showing dislocations within austenite. (d) TEM image from thermal cycling of 50.4% Ni NiTi in [1 2 3] orientation 1 cycle at each + 25 MPa increment from +0 MPa to +100 MPa with RT → −100 °C → 100 °C → RT. (e) TEM image from thermal cycling of solutionized 50.4% Ni NiTi [0 0 1] orientation with the following history: 1 cycle @ +125 MPa, +140 MPa, +170 MPa, +185 MPa, +215 MPa, +230 MPa, +245 MPa, +260 MPa; 2 cycles @ +200 MPa; 3 cycles @ +155 MPa. (f) Dislocation slip at room temperature of a solutionized Ti–50.8 at.% Ni [0 0 1] single crystal. Prior to TEM, the specimen was strained to 10% at room temperature (≈25 °C).

Please cite this article in press as: Ezaz T et al. Plastic deformation of NiTi shape memory alloys. Acta Mater (2012), http://dx.doi.org/10.1016/j.actamat.2012.09.023

The deformed samples are interrogated with transmission electron microcopy (TEM) upon conclusion of the pseudoleastic deformation response. Fig. 3 shows TEM micrographs of dislocation arrangements observed at the same spot in the specimen deformed at room temperature. The Burgers vector of dislocations marked with the letter A (colored black) in Fig. 3a is identified to be [0 1 0] from *g.b* analysis. By contrast, the dislocations marked with the letter B (colored black) in Fig. 3b have a Burgers vector $[1\,\bar{1}\,1]$. These dislocations tangle with each other, which is a cause of high strain hardening observed during deformation. To our knowledge, this is the first evidence of the presence of the $[1\,\bar{1}\,1]$ dislocations in NiTi. We note that these dislocations are not inherited from martensite as the corresponding plane in martensite ($(0\,0\,1)_M$ plane) is not a slip plane [17].

2.2. Further evidence of dislocation slip in thermal cycling and pseudoelasticity experiments at the microscale

Strong evidence of slip is noted in NiTi alloys of different compositions in early work which is summarized in Ref. [20]. Typical Ni-rich compositions studied in our work on single crystals are in the range 50.1 to 50.8% Ni. A series of strain–temperature responses were given in Ref. [20] and they conform to the pattern shown in Fig. 1a. TEM results from these experiments under temperature cycling (under stress) are shown in Fig. 4a–f. In all cases, the slip activity in the austenite phase is noted. When austenite-to-martensite interfaces are shown, it is noted that the dislocations exist primarily in the austenitic phase. In the case of 50.1% and 50.4% Ni NiTi compositions the temperature is cycled from RT → −100 °C → 100 °C → RT under stress. In Fig. 4a, the martensite and austenite domains are marked; in Fig. 4b, the lower half of the image shows the transformation-induced dislocations in the austenitic phase, and the upper half shows the martensite. In Fig. 4c–e the dislocation configurations in the austenite away from the austenite–martensite interface are shown. In the case of solutionized 50.8% Ni and higher Ni compositions the martensite start and finish temperatures are all below −100 °C, hence the deformation is conducted in the pseudoelastic regime above austenite finish temperature as noted in Fig. 4f.

2.3. Plasticity mediated transformation strains and residual strains under thermal cycling at the macroscale

The results of differential scanning calorimetry for NiTi are shown in Fig. 5a and the shape memory strains via temperature cycling under stress are shown in Fig. 5b for 50.1% Ni. The strain for the correspondent variant pair CVP formation and CVP+ detwinning strain from theory are marked in Fig. 5b. This experiment is conducted on a single crystal with the loading axis in the [1 2 3] direction. The detwinning strain in tension is appreciable and increases the maximum transformation strains depending on the crystal orientation. The main reason why the theoretical strain levels (10.51%) are not reached is the occurrence of slip resulting in irreversibility. The plastic strain is noted at the maximum temperature end of the strain–temperature curves as the stress level exceeds 125 MPa.

3. Simulation methodology: GSFE calculations

The energy barrier during dislocation motion in a glide system is established via generalized stacking fault energy (GSFE) [30]. Also referred to as the fault energy curve, GSFE is defined as the energy associated with a rigid shift of the upper elastic half space with respect to the lower half

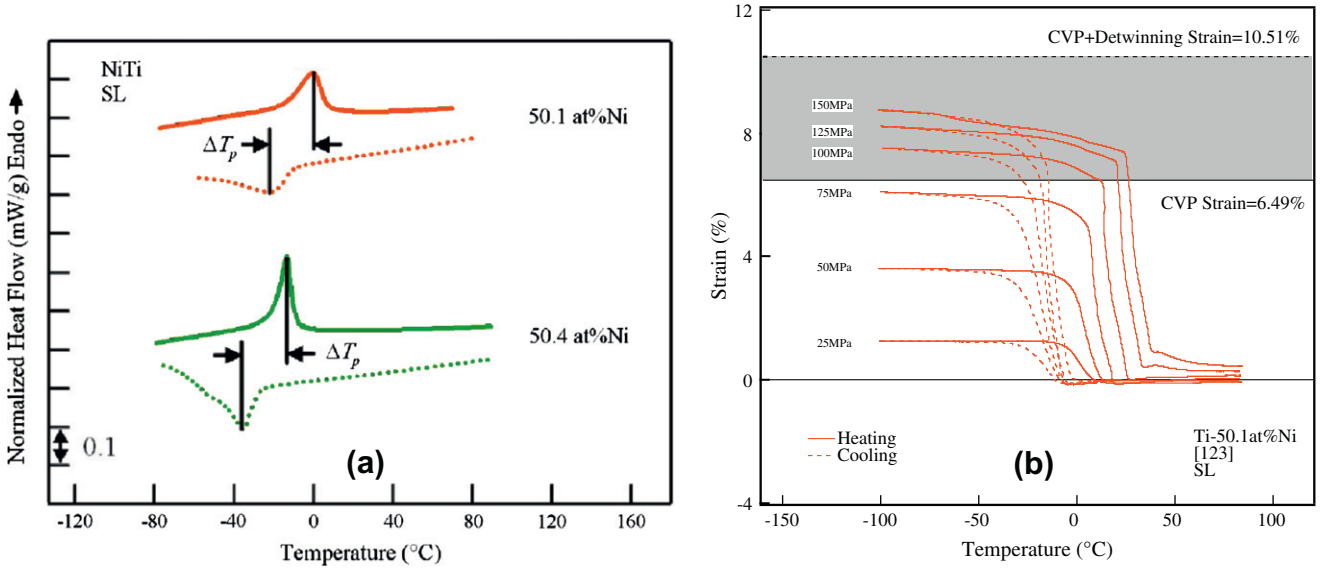

Fig. 5. (a) Differential scanning calorimetry results for solutionized 50.1% Ni–Ti and 50.4% Ni–Ti; the dotted curve is for cooling, and the hysteresis levels are also marked on the figures [32]. (b) Strain–temperature curves under temperature cycling showing the buildup of plastic strain with increase in stress (adapted from Ref. [18]).

Please cite this article in press as: Ezaz T et al. Plastic deformation of NiTi shape memory alloys. Acta Mater (2012), http://dx.doi.org/10.1016/j.actamat.2012.09.023

on a given slip plane in a given slip direction. During a GSFE calculation, a complete landscape of fault energy is investigated, which requires a displacement of a repeating unit lattice in the respective shear direction. Hence, the total displacement magnitudes in [1 0 0] and [1 $\bar{1}$ 1] directions are a and $a[1\,\bar{1}\,1] = \sqrt{3}a$ respectively. The GSFE for the slip system $[u\,v\,w](h\,k\,l)$ is plotted against the displacement in each layer, u_x, which is normalized by its respective displacement, $\|[u\,v\,w]\|$.

We used spin-polarized, ab initio calculation to properly determine the undeformed and deformed energy states of NiTi austenite during the shearing in a certain slip system. The ab initio calculations were conducted via the density functional theory based Vienna Ab initio Simulation Package (VASP) [32] and the generalized gradient approximation (GGA) [33] is implemented on a projection-augmented wave (PAW). Monkhorst–Pack $9 \times 9 \times 9$ k-point meshes were used for Brillouin zone integration. The structural parameter of NiTi in the B2 phase was calculated first and found to be 3.004 Å with a stable energy of −6.95 eV per atom. We have used an L-layer $(h\,k\,l)$-based cell to calculate defect energies and performed shear along the $[u\,v\,w]$ direction to generate the GSFE curve in that system. We assessed the convergence of the GSFE energies with respect to increasing L, which indicates that the fault energy interaction in adjacent cells due to periodic boundary conditions will be negligible. The convergence is ensured once the energy calculations for L and L + 1 layers yield the same GSFE.

The calculation of GSFE was followed up by incorporating a displacement of known magnitude (as discussed above) and performing a full internal atom relaxation, including perpendicular direction to the glide planes, until the atomic forces were less than ±0.020 eV Å^{-1}. Further details of the computational method can be obtained in earlier literature [34].

4. Simulation results

4.1. The (0 1 1)[1 0 0], (0 1 1)[1 $\bar{1}$ 1] and (0 1 1)[0 $\bar{1}$ 1] systems

4.1.1. The (0 1 1)[1 0 0] case

This is the most observed slip system in austenitic NiTi. In the B2 NiTi crystal structure, in the [0 1 1] stacking direction, in plane Ni (Ti) and out-of-plane Ni (Ti) atoms are periodically arranged (stacking sequence ABAB…) as shown in Fig. 6a. The atom positions during shearing are shown in Fig. 6b and c. The maximum energy barrier in this system is found to be 142 mJ m^{-2} (shown in Fig. 6d). The dislocations need to glide a distance a in the [1 0 0] direction to preserve the same stacking sequence. After a glide of a distance $a/2$ [1 0 0], the in plane Ni and in plane Ti reach the shortest near neighbor distance, which is shown in Fig. 6b. This point corresponds to "unstable fault energy". After a sliding distance of $a/4$ ($u_x/a[1\,0\,0] = 0.25$) and a distance of $3a/4$ ($u_x/a[1\,0\,0] = 0.75$) (antiphase of $a/4$ ($u_x/a[1\,0\,0] = 0.25$)), the atomic positions of the first shear layer (shown by the green box in Fig. 6c) are different, which results in an asymmetrical shape for the GSFE. Specifically, for the ($u_x/a[1\,0\,0] = 0.75$) case (Fig. 6c) the Ni atoms are positioned over other nickel atoms (near neighbors), which raises the energy levels. On the other hand, at $u_x/a[1\,0\,0] = 0.25$ the Ni atoms are positioned over Ti atoms in the next layer and the corresponding energy level is lower.

4.1.2. The (0 1 1)[1 $\bar{1}$ 1] case

The energetics of the (0 1 1)[1 $\bar{1}$ 1] slip system is calculated and shown in Fig. 7. We reported the occurrence of slip in this system in this study in Fig. 5b. The stacking sequence is ABAB… where the cell repeats every two planes in the [0 1 1] direction. In Fig. 7a, we show all the atoms and designate the furthest out-of-plane layer as (6) and the layer on the plane of the paper as in-plane (1). Atoms between layers 1 and 6 are shown with various diameters to indicate their position with respect to layers 1 and 6. The atom positions at $\sqrt{3}a/3(u_x/a|[1\,\bar{1}\,1]| = 0.33)$ and $\sqrt{3}a/2(u_x/a|[1\,\bar{1}\,1]| = 0.5)$ are shown in Fig. 7b and c, respectively. During sliding of the upper block of atoms relative to the lower half, the fault energy curve follows the typical antiphase boundary (APB) energy profile and is symmetric at the midpoint, $u_x/a|[1\,\bar{1}\,1]| = 0.5$ (shown in Fig. 7d). The fault energy reaches a maximum (660 mJ m^{-2}) after a sliding distance $\sqrt{3}a/3(u_x/a|[1\,\bar{1}\,1]| = 0.33)$ (shown in Fig. 7d) and $2\sqrt{3}a/3(u_x/a|[1\,\bar{1}\,1]| = 0.67)$. At this position, near neighbor distances of two similar atoms (Ni or Ti) become the shortest. At $\sqrt{3}a/2(u_x/a|[1\,\bar{1}\,1]| = 0.50)$, a slightly lower peak of 515 mJ m^{-2} is observed where the near neighbor distance of two dissimilar atoms becomes the shortest.

4.1.3. The (0 1 1)[0 $\bar{1}$ 1] case

The (0 1 1)[0 $\bar{1}$ 1] system has been analyzed and the atom positions and the GSFE curve are shown in Fig. 8. In the B2 structure, Ni and Ti atoms are periodically arranged (stacking sequence is ABAB… as shown in Fig. 8a). Therefore, dislocations need to glide a distance $\sqrt{2}a$ in the [0 $\bar{1}$ 1] direction to obtain the same stacking sequence. After a glide of a distance $\sqrt{2}a/2$, the Ni or Ti atoms reach the shortest near neighbor distance shown in Fig. 8b. The maximum barrier energy in this system is found to be very high, at 1545 mJ m^{-2} (shown in Fig. 8c). Based on these results, (0 1 1)[0 $\bar{1}$ 1] slip can occur at very high stress levels as we discuss later.

4.2. The ($\bar{2}$ 1 1)[1 1 1] and (0 0 1)[0 1 0] systems

4.2.1. The ($\bar{2}$ 1 1)[1 1 1] case

The ($\bar{2}$ 1 1)[1 1 1] is a possible slip system in body centered cubic (bcc) metals. The GSFE curve for the ($\bar{2}$ 1 1) plane in the [1 1 1] direction is calculated by shearing the ($\bar{2}$ 1 1) top half elastic space relative to the bottom in the [1 1 1] direction, as shown in Fig. 9a. The viewing direction is [0 $\bar{1}$ 1]. The GSFE in this system is plotted in Fig. 9d. The plot reveals two distinct features for this system: (i) there is

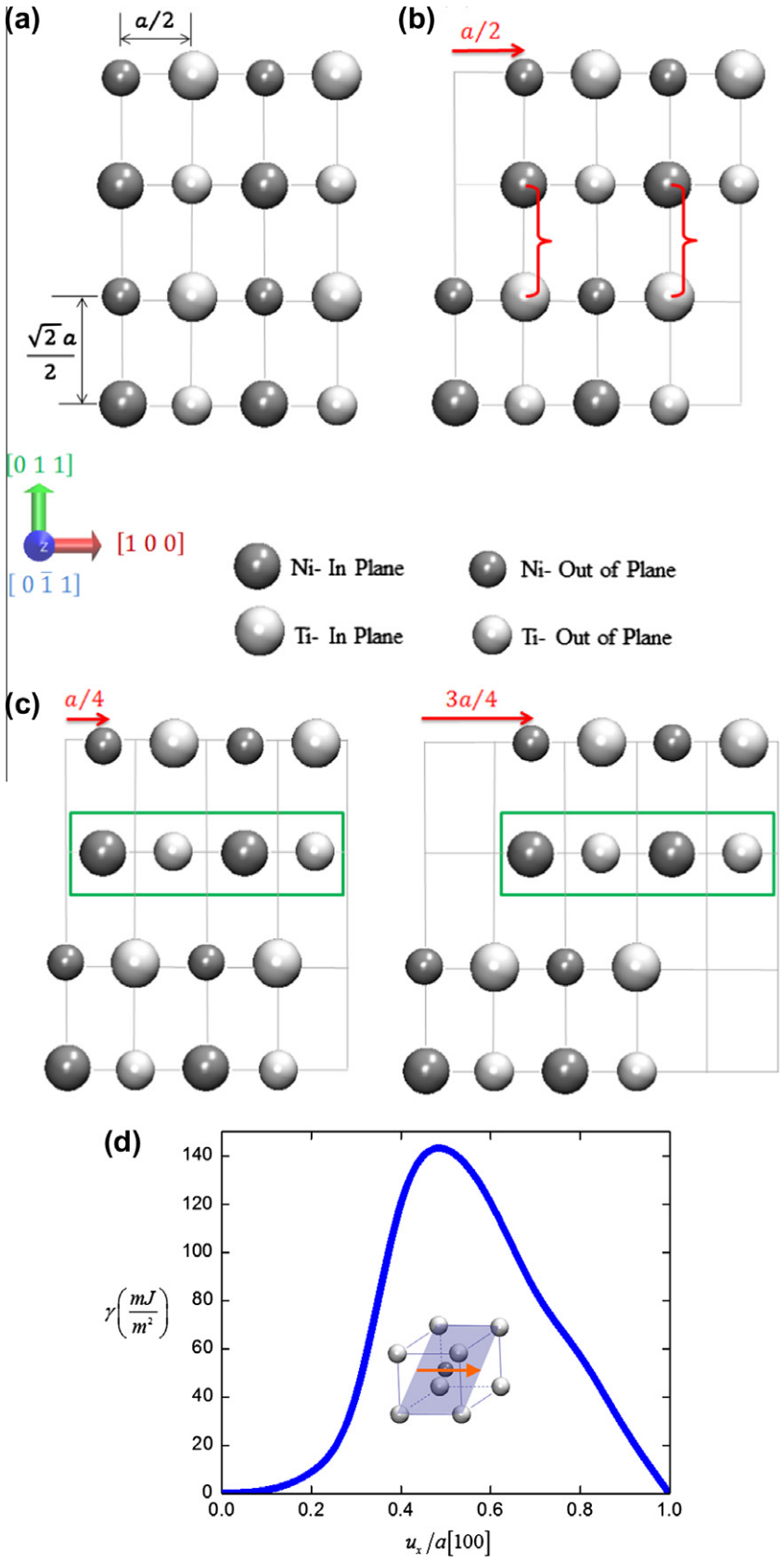

Fig. 6. (a) Crystal structure of B2 NiTi observed from the $[0\bar{1}1]$ direction. (b) After a rigid displacement of $a/2$ ($u_x/a[100] = 0.5$), the near neighbor distance of two in-plane Ni or Ti atoms becomes shortest (shown by red parenthesis). (c) After displacements of $a/4$ ($u_x/a[100] = 0.25$) and $3a/4$ ($u_x/a[100] = 0.75$). The position of atoms of the first shear layer (shown by the green box) with respect to the undeformed lower half is different. (d) GSFE curve for the $(011)[100]$ system. (For interpretation of the references to colour in this figure legend, the reader is referred to the web version of this article.)

Please cite this article in press as: Ezaz T et al. Plastic deformation of NiTi shape memory alloys. Acta Mater (2012), http://dx.doi.org/10.1016/j.actamat.2012.09.023

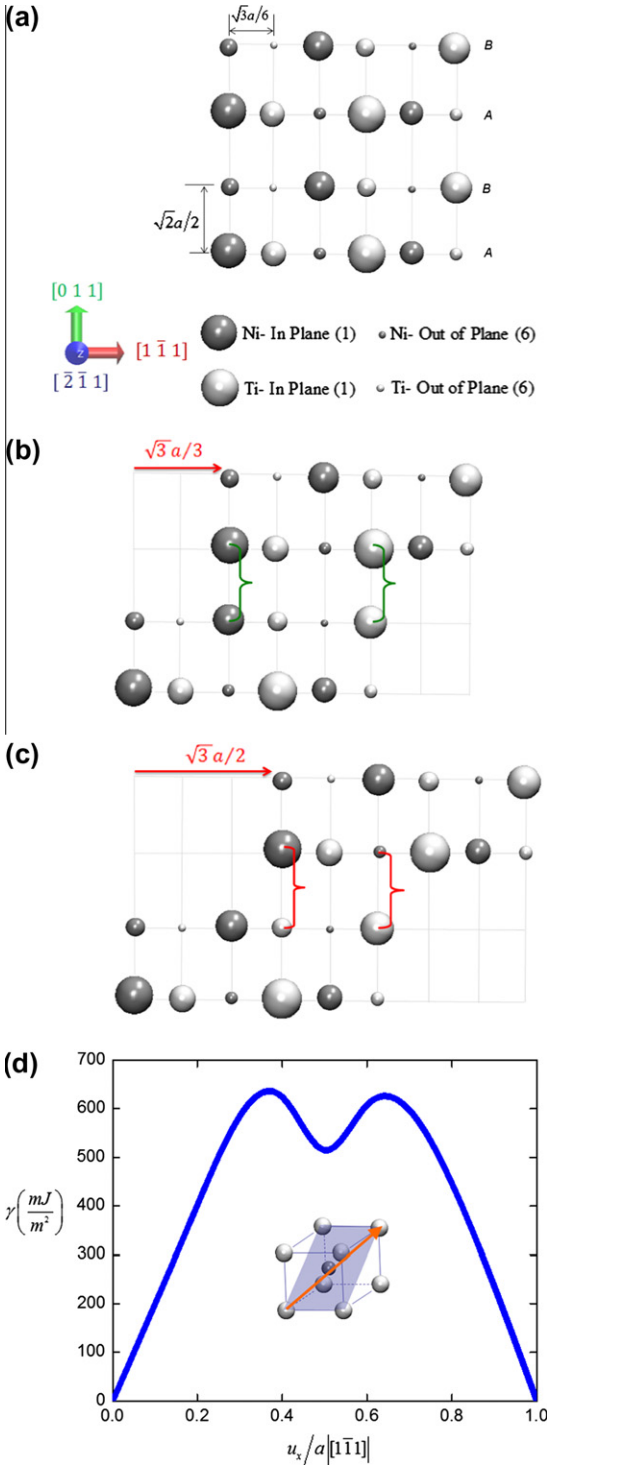

Fig. 7. (a) Crystal structure of B2 NiTi observed from the $[\bar{2}\,1\,1]$ direction. Stacking sequence in the $[0\,1\,1]$ direction is shown as ABAB. (b) After a rigid displacement of $\sqrt{3}a/3(u_x/a|[1\,\bar{1}\,1]| = 0.33)$, the near neighbor distance of two out-of-plane Ni or Ti atoms becomes shortest (shown by green parenthesis). (c) After a displacement of $\sqrt{3}a/2(u_x/a|[1\,\bar{1}\,1]| = 0.5)$ near neighbor distance of out-of-plane Ni (Ti) and Ti (Ni) atoms becomes shortest (shown by red parenthesis), and the anti-phase boundary induced by slip alters the stacking of Ni and Ti atoms). (d) GSFE curve for the $(0\,1\,1)[1\,\bar{1}\,1]$system. (For interpretation of the references to colour in this figure legend, the reader is referred to the web version of this article.)

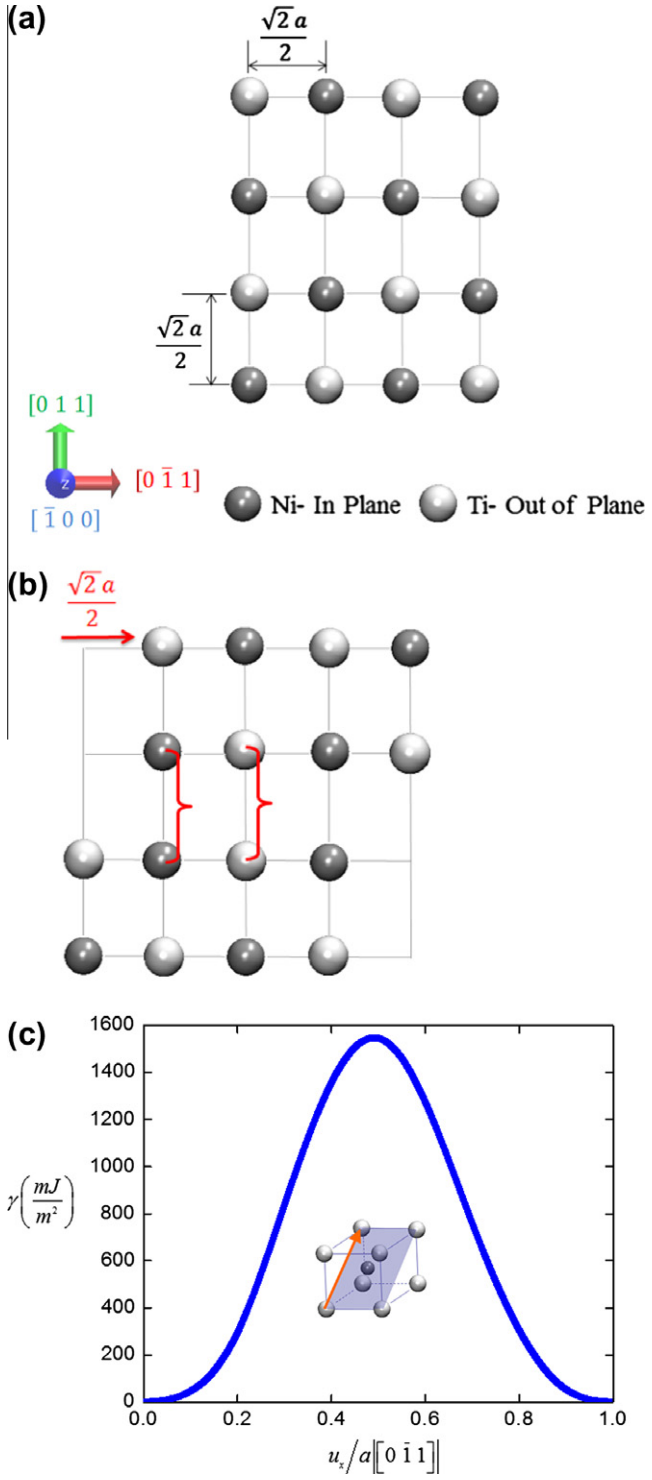

Fig. 8. (a) Crystal structure of B2 NiTi observed from the $[\bar{1}\,0\,0]$ direction. (b) After a rigid displacement of $\sqrt{2}a/2(u_x/a|[0\,\bar{1}\,1]| = 0.5)$, the near neighbor distance of two in-plane Ni or Ti atoms becomes shortest (shown by red parenthesis). (c) GSFE curve for system $(0\,1\,1)[0\,\bar{1}\,1]$. (For interpretation of the references to colour in this figure legend, the reader is referred to the web version of this article.)

a metastable position at the midpoint of a displacement of $\sqrt{3}a/2$ $(u_x/a[\![1\,1\,1]\!] = 0.5)$, (ii) the energy barriers for dislocation glide in the $[1\,1\,1]$ and $[\bar{1}\,\bar{1}\,\bar{1}]$ directions are unequal.

Please cite this article in press as: Ezaz T et al. Plastic deformation of NiTi shape memory alloys. Acta Mater (2012), http://dx.doi.org/10.1016/j.actamat.2012.09.023

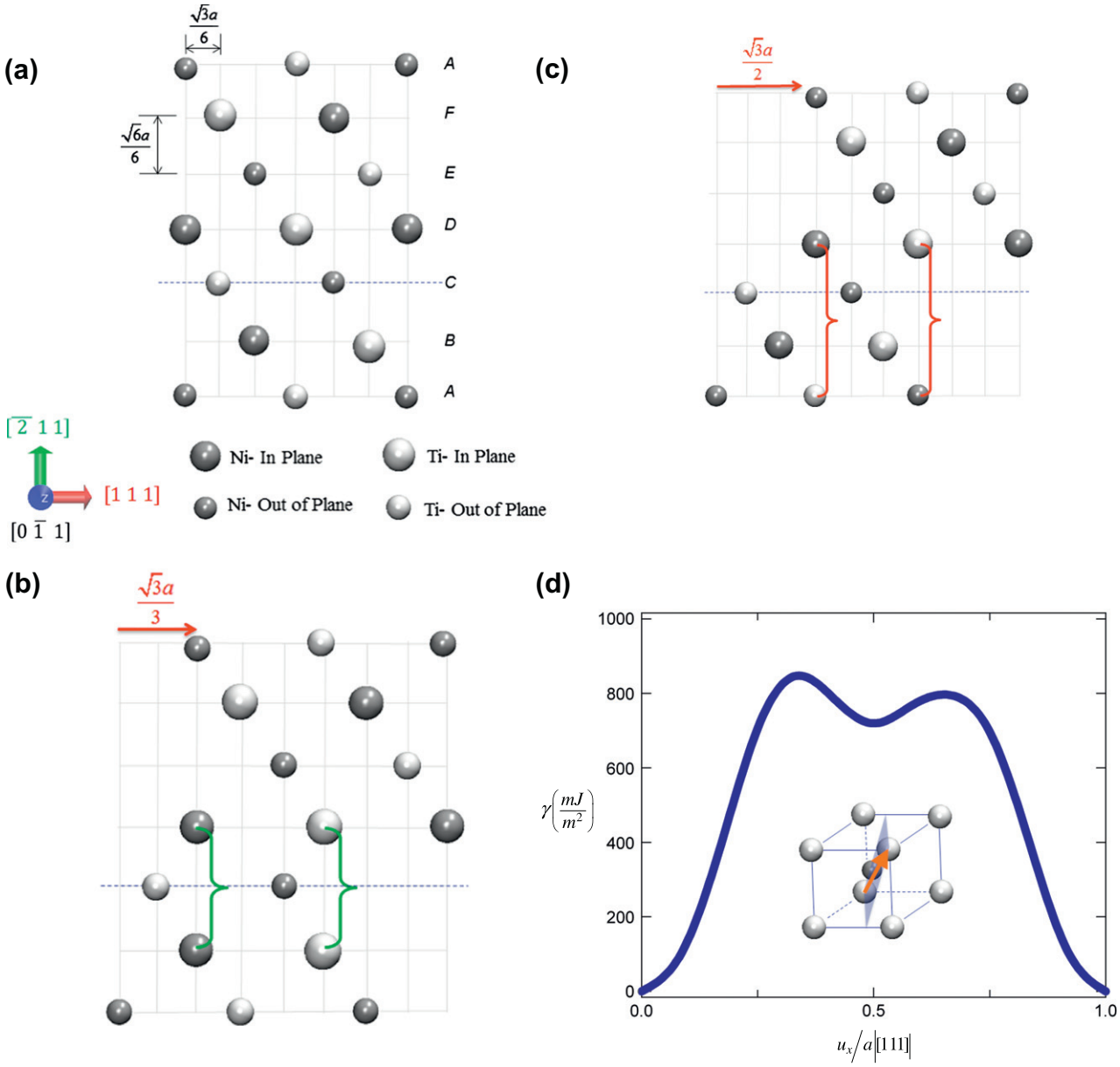

Fig. 9. (a) Crystal structure of B2 NiTi observed from the $[0\bar{1}1]$ direction. The stacking sequence is ABCDEFA, where the cell repeats every six planes in the $[\bar{2}11]$ direction and the dashed line denotes the slip plane. (b) After a rigid displacement of $\sqrt{3}a/3(u_x/a|[111]| = 0.33)$, the near neighbor distance of two in-plane Ni or Ti atoms is shortest (shown by red parenthesis). (c) After a rigid displacement of $\sqrt{3}a/2(u_x/a|[111]| = 0.5)$, near neighbor distance of in-plane Ni and out-of-plane Ti atoms is largest (shown by red parenthesis). (d) GSFE curve for the $(\bar{2}11)[111]$ system. (For interpretation of the references to colour in this figure legend, the reader is referred to the web version of this article.)

The maximum energy barrier is calculated to be 847 mJ m^{-2} at position $u_x/a|[111]| = 0.33$. At this position the near neighbor distance between two Ni or Ti atoms becomes the shortest. A metastable position is observed at $u_x/a|[111]| = 0.5$, which lowers the energy by 155 mJ m^{-2} to 692 mJ m^{-2}. A second peak is observed at $u_x/a|[111]| = 0.67$ with 795 mJ m^{-2}.

4.2.2. The (001)[010] case

Another possible slip system for the bcc structure is (001)[010] and is also investigated for B2 NiTi. In the B2 structure, Ni and Ti atoms are symmetrically arranged in the [001] and [010] direction, which is shown in Fig. 10a. During shearing in this system, in plane Ni and out-of-plane Ti atoms get nearer only at a position $a/2$ $(u_x/a|[010]| = 0.5)$ (shown in Fig. 10b). The GSFE curve shown in Fig. 10c exhibits only one peak pointing out this position. The maximum energy barrier for atoms to glide in (001) in [100] direction is calculated to be 863 mJ m^{-2}.

5. Analysis and discussion of results

The importance of slip in influencing the shape memory alloy characteristics is well known and further illustrated

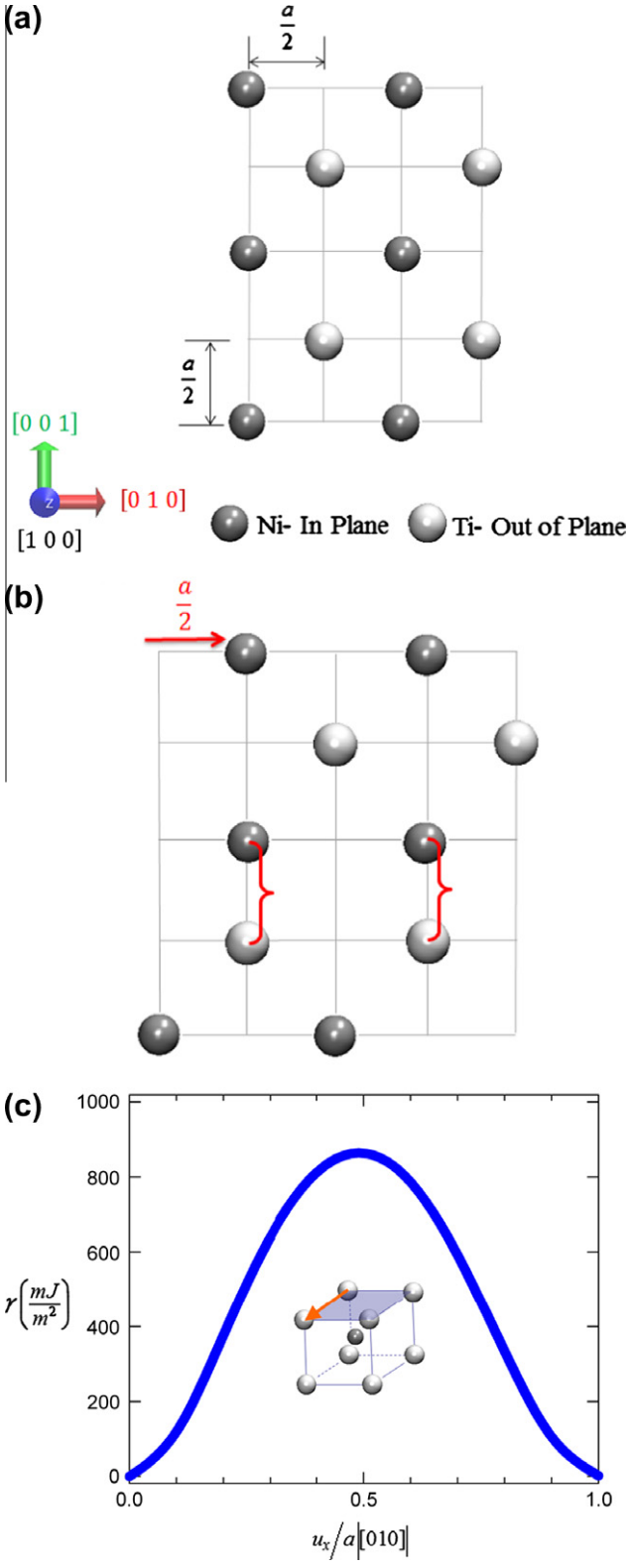

Fig. 10. (a) Crystal structure of B2 NiTi observed from the [1 0 0] direction. (b) After a rigid displacement of a/2 ($u_x/a|[0\,1\,0]| = 0.5$), the near neighbor distance of in-plane Ni and out-of-plane Ti atoms becomes shortest (shown by red parenthesis). (b) GSFE curve for the (0 0 1)[0 1 0] system. (For interpretation of the references to colour in this figure legend, the reader is referred to the web version of this article.)

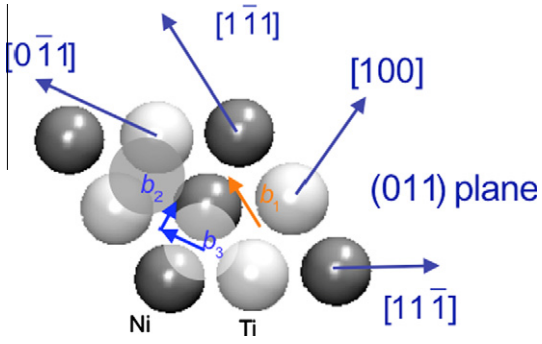

Fig. 11. Decomposition of $[1\,\bar{1}\,1]$ slip (b_1) along $[0\,\bar{1}\,1]$ (b_3) and [1 0 0] (b_2) directions. The slip plane shown is (0 1 1). Ni atoms are denoted by the dark shading in this schematic. (For interpretation of the references to colour in this figure legend, the reader is referred to the web version of this article.)

based on the TEM images given in Fig. 3 and 4. The observation of $(0\,1\,1)[1\,\bar{1}\,1]$ slip in Fig. 3b is particularly noteworthy (and the first to our knowledge).

Although some of the shape memory materials have high theoretical transformation strains such as the Cu-based alloys [35] and Fe-based alloys [36,37], their performance has not been as favorable because of the occurrence of plastic deformation. The NiTi alloys have been widely accepted as having superior performance characteristics because of their inherent resistance to slip. The present work explains the origins of the high resistance to slip in NiTi alloys.

In B2 NiTi, slip systems such as $(\bar{2}\,1\,1)[1\,1\,1]$ or (0 0 1) [0 1 0] have significantly higher fault barrier energy as compared to the $(0\,1\,1)[1\,0\,0]$ and $(0\,1\,1)[1\,\bar{1}\,1]$ systems. Thus, in B2 NiTi, dislocation glide is more likely in the $(0\,1\,1)[1\,0\,0]$ and $(0\,1\,1)[1\,\bar{1}\,1]$ systems.

The $[1\,\bar{1}\,1]$ dislocation can dissociate into partial dislocations with smaller Burgers vectors. According to Frank's energy criteria, an $a[1\,\bar{1}\,1]$ dislocation can dissociate into two $a/2[1\,\bar{1}\,1]$ partial dislocations:

$$a[1\,\bar{1}\,1] \rightarrow \frac{a}{2}[1\,\bar{1}\,1] + \frac{a}{2}[1\,\bar{1}\,1] \tag{1}$$

This kind of dissociation has been reported for FeAl or CuZn [38]. In the ordered NiTi, an energy well is present in the $(0\,1\,1)[1\,\bar{1}\,1]$ GSFE curve at $u_x/a|1\bar{1}1| = 0.5$ (Fig. 7d), confirming the presence of an APB. Hence, dislocations present in the $(0\,1\,1)[1\,\bar{1}\,1]$ system can dissociate into partial dislocations with a stable equilibrium distance. We note that the separation distance would be rather small in view of the high APB energy and the resolved stress required would need to be rather high to move these dislocations.

The $[1\,\bar{1}\,1]$ dislocations can decompose into perfect dislocations on the (0 1 1) plane. Hence, as illustrated in Fig. 11, a $[1\,\bar{1}\,1]$ dislocation dissociates according to Eq. (2). In Fig. 11, b_2, b_3 represent the dissociated dislocations.

$$\begin{aligned} &a[1\,\bar{1}\,1] \rightarrow a[1\,0\,0] + a[0\,\bar{1}\,1] \\ &b_1 \rightarrow b_2 + b_3 \end{aligned} \tag{2}$$

Table 1
Maximum fault energy, shear modulus and elastic energy in different possible slip systems in B2 NiTi. The fault energy (computational) tolerance is less than 0.17 mJ m^{-2}.

Slip plane	Burgers vector $\bar{b}$	Maximum fault energy (mJ m^{-2})
(0 1 1)	[1 0 0]	142
(0 1 1)	[1 $\bar{1}$ 1]	660
(0 1 1)	[0 $\bar{1}$ 1]	1545
($\bar{2}$ 1 1)	[1 1 1]	847
(1 0 0)	[0 1 0]	863

Table 2
Slip elements in B2 NiTi. The calculated (ideal) critical stress for slip is given in the last column. The critical stress tolerance is less than 2.25 MPa.

Slip plane	Slip direction	$(\tau_{shear})_{ideal} = \frac{\delta\gamma}{\delta u_x}\Big\vert_{\max}$ (MPa)
(0 1 1)	[1 0 0]	2667
(0 1 1)	[1 $\bar{1}$ 1]	5561
(0 1 1)	[0 $\bar{1}$ 1]	12,847
($\bar{2}$ 1 1)	[1 1 1]	7430
(1 0 0)	[0 1 0]	9320

The b_3 dislocation may further decompose to yield additional ⟨1 0 0⟩ type perfect dislocations:

$$a[0\,\bar{1}\,1] \rightarrow a[0\,\bar{1}\,0] + a[0\,0\,1] \quad (3)$$

Based on the simple Frank's rule, there is no change in elastic energy associated with Eqs. (2) and (3) as noted first by Nabarro [39]. And a resolved stress that acts favorably on the a[1 0 0] can move this dislocation independently of others. This is particularly true in view of the lower GSFE magnitudes for the a[1 0 0] case. Therefore, the [1 $\bar{1}$ 1] or even [0 $\bar{1}$ 1] dislocations could exist in the crystal, but they do not dominate the dislocation slip process because they decompose, under sufficient stress, to yield ⟨1 0 0⟩ dislocations.

In the case of austenitic NiTi, ⟨1 1 1⟩ or ⟨1 0 0⟩ slip are identified as noted in Fig. 3. Two factors are noteworthy. The first is that the B2 NiTi maintains a strong directionality in its Ni–Ni, Ti–Ti and Ni–Ti bonds; hence, a covalent bonding nature is observed in its deformation characteristics [40]. This covalent nature influences the energy levels observed during the entire simulations. The second factor is that the interplanar distance between the {1 1 2} plane is measured to be 1.23 Å, whereas between {0 1 1}, this is calculated to be 2.13 Å. Shearing of covalent bonds with smaller interplanar distance requires higher stresses and is manifested by a higher maximum fault energy.

The magnitude of maximum fault energy indicates the most energetically favorable system for dislocation nucleation [41,42] and the slope of the GSFE curve equivalently measures the slip nucleation stress as follows: $(\tau_{shear})_{ideal} = \delta\gamma/\delta u_x|_{\max}$ [43,44]. Hence, in a cubic system, with a single family of slip systems, the maximum energy barrier and ideal slip nucleation stress has a one-to-one correlation with each other and unstable stacking fault energy γ_{us} can be utilized to point out the active slip systems. In the case of a cubic system with multiple slip systems, the slip vector needs to be accounted for the calculation of ideal stress as well. The results shown in Table 1 utilize both the γ_{us} values and the corresponding Burgers vector for different slip systems in the calculation of ideal stress. Also, we note that ideal slip nucleation stress calculated from the GSFE of a particular system accounts for the anisotropy of the system and a measure without any continuum approximation. However, ideal nucleation stress differs from actual since the energy associated with the creation of a surface during dislocation emission and effects related to reconstruction of the dislocation core are neglected, which contributes to actual Peierls stress. These approximations may affect the exact number, but we expect the qualitative picture to remain the same.

It is important to point out that the unstable stacking fault energy for the (0 1 1)[1 0 0] is 142 mJ m^{-2} which is significantly lower than for pure metals and B19' martensite [34]. Consequently, slip in the B2 system is favored compared to martensite (B19') slip as noted in Figs. 3a and b and Fig. 5. The (0 1 1)[1 0 0] system will be activated at 2.6 GPa and the (0 1 1)[1 $\bar{1}$ 1] system is expected to be activated at ideal stresses exceeding 5 GPa (Table 2). These levels represent ideal stresses and in experiments, local stresses in the vicinity of martensites [45], or near precipitates can be significant in mediating dislocation slip plasticity. In the analysis of Norfleet, the most stressed slip systems upon stress-induced transformation exceeded 2500 MPa, triggering local slip in austenite [9]. Also, experiments on nanopillars confirm that plastic deformation initiated in austenite at stress levels exceeding 2.5 GPa [46].

Returning to the GSFE of the ($\bar{2}$ 1 1)[1 1 1] system, as noted earlier, the energetic barrier for dislocation glide is higher than for (0 1 1)[1 $\bar{1}$ 1] or (0 1 1)[1 0 0]. Hence, in B2 NiTi, dislocation glide in this system is possible only when the Schmid factor associated with internal stresses provides a large contribution. A metastable position is observed at $u_x/a|[1\,1\,1]| = 1/2$ in this system. However, to nucleate any $a/2$[1 1 1] superpartial, the atoms have to overcome an energy barrier of 847 mJ m^{-2} with a shear of 2.12. However, the energetic profile of ($\bar{2}$ 1 1)[1 1 1] is important since twinning glide can occur in this system. A perfect [1 1 1] dislocation can dissociate into three $a/3$[1 1 1] superpartials that glide in three consecutive planes and generate a three layer twin [7,47]. The energy barrier during (1 1 2) twinning has recently been calculated [48].

The study sheds light on whether to-and-fro APB dragging can be a possible mechanism for shape memory. The concept is intriguing; under stress or temperature changes, the (0 1 1)[1 $\bar{1}$ 1] dislocation motion could undergo reversible motion. Such a mechanism could potentially explain cases where the material undergoes nearly complete recovery despite the presence of dislocations in the micrographs. We note the need for further research in this particular area.

6. Summary

Further advances towards a quantitative understanding of slip in austenitic NiTi have been achieved. The results

explain, in light of the generalized stacking fault energy (GSFE) curves, why mainly $(0\,1\,1)[1\,0\,0]$ and $(0\,1\,1)[1\,\bar{1}\,1]$ systems are observed in experiments, and we provide a rationale for slip resistance in NiTi austenite with our predictions.

As shown in Table 2, the magnitude of ideal stress required for dislocation slip is determined to exceed 2 GPa. The reversible transformation can occur without dislocation build-up provided that transformation stress magnitudes are limited to levels less than required to activate slip. This is indeed the case for the NiTi alloys; further improvement of slip resistance is important because the TEM evidence points to activation of slip in pseudoelastic and shape memory cases. The present results emphasize the importance of understanding of the atomic displacements and metastable positions (APBs) in most important slip systems. Overall, the study represents a methodology for consideration of a better understanding of shape memory alloys.

Acknowledgements

The work is supported by the National Science Foundation under DMR-0803270. The authors gratefully acknowledge the use of the parallel computing resources part of the Taub cluster provided by the Computational Science and Engineering Program at the University of Illinois, partial support from CMMI-09-26813 and CRDF Award RUE1-2983-TO-10. The assistance of Wael Abuzaid with the pseudoelasticity experiments is acknowledged.

References

[1] Olson GB, Cohen M. Scripta Mater 1975;9:1247.
[2] Gall K, Sehitoglu H. Int J Plast 1999;15:69.
[3] Melton KN, Mercier O. Acta Metall 1979;27:137.
[4] Miyazaki S, Imai T, Igo Y, Otsuka K. Metall Trans A 1986;17A:115.
[5] Strnadel B, Ohashi S, Ohtsuka H, Ishihara T, Miyazaki S. Mater Sci Eng A 1995;202:148.
[6] Delaey L, Krishnan RV, Tas H, Warlimont H. J Mater Sci Lett 1974;9:1521.
[7] Surikova NS, Chumlyakov YI. Phys Met Metallogr 2000;89:196.
[8] Simon T, Kroger A, Somsen C, Dlouhy A, Eggeler G. Acta Mater 2010;58:1850.
[9] Norfleet DM, Sarosi PM, Manchiraju S, Wagner MFX, Uchic MD, Anderson PM, et al. Acta Mater 2009;57:3549.
[10] Pelton AR, Huang GH, Moine P, Sinclair R. Mater Sci Eng A 2012;532:130.
[11] Kibey S, Sehitoglu H, Johnson DD. Acta Mater 2009;57:1624.
[12] Sanati M, Albers RC, Pinski FJ. Phys Rev B: Condens Matter 1998;58:13590.
[13] Xiangyang H, Ackland GJ, Rabe KM. Nat Mater 2003;2:307.
[14] Wagner MFX, Windl W. Acta Mater 2008;56:6232.
[15] Hatcher N, Kontsevoi OY, Freeman AJ. Phys Rev B: Condens Matter 2009;80:144203.
[16] Ezaz T, Sehitoglu H. Appl Phys Lett 2011;98:141906.
[17] Ezaz T, Sehitoglu H, Maier HJ. Acta Mater 2011;59:5893.
[18] Tyumentsev AN, Surikova NS, Litovchenko IY, Pinzhin YP, Korotaev AD, Lysenko OV. Acta Mater 2004;52:2067.
[19] Moberly WJ, Proft JL, Duerig TW, Sinclair R. Acta Mater 1990;38:2601.
[20] Hamilton RF, Sehitoglu H, Chumlyakov Y, Maier HJ. Acta Mater 2004;52:3383.
[21] Delaey L, Ortin J, VanHumbeeck J. Inst Met 1988;60.
[22] Van Humbeeck J, Aernoudt E, Delaey L, Lu L, Verguts H, Ortin J. Rev Phys Appl 1988;23:557.
[23] Delville R, Malard B, Pilch J, Sittner P, Schryvers D. Int J Plast 2011;27:282.
[24] Duerig TW. Mater Sci Eng A 2006;438–440:69.
[25] Kelly A, Groves GW, Kidd P. Crystallography and crystal defects. New York: Wiley; 2000.
[26] Taylor GI. Proc Roy Soc A 1934;145:362.
[27] Ardley GW, Cottrell AH. Proc Roy Soc A 1953;219:328.
[28] Stoloff NS, Davies RG. Acta Metall 1964;12:473.
[29] Rachinger WA, Cottrell AH. Acta Metall 1956;4:109.
[30] Vitek V. Philos Mag 1968;18:773.
[31] Wagoner AJ, Hamilton RF, Sehitoglu H, Biallas G, Maier HJ, Chumlyakov YI, et al. Metall Mater Trans A 2005;36A:919.
[32] Kresse G, Hafner J. Phys Rev B: Condens Matter 1993;48:13115.
[33] Perdew JP, Burke K, Ernzerhof M. Phys Rev Lett 1996;77:3865.
[34] Kibey S, Liu JB, Johnson DD, Sehitoglu H. Acta Mater 2007;55:6843.
[35] Sade M, Rapacioli R, Ahlers M. Acta Metall 1985;33:487.
[36] Kajiwara S. Mater Sci Eng A 1999;273:67.
[37] Sehitoglu H, Zhang XY, Kotil T, Canadinc D, Chumlyakov Y, Maier HJ. Metall Mater Trans A 2002;33:3661.
[38] Potter DI. Mater Sci Eng 1970;5:201.
[39] Nabarro F. Adv Phys 1952;1:269.
[40] Wang F. Bonding theory of metals and alloys. Oxford: Elsevier; 2005.
[41] Rice JR, Beltz GE. J Mech Phys Solids 1994;42:333.
[42] Rice JR. J Mech Phys Solids 1992;40:239.
[43] Juan Y-M, Kaxiras E. Philos Mag A 1996;74:1367.
[44] Ogata S, Li J, Yip S. Science 2002;298:807.
[45] Sun QP, Hwang KC. J Mech Phys Solids 1993;41:1.
[46] Frick CP, Orso S, Arzt E. Acta Mater 2007;55:3845.
[47] Moberly WJ. PhD thesis, Stanford University; 1991.
[48] Ezaz T, Sehitoglu H. Appl Phys Lett 2011;98:241906.